

Jet production in two-photon collisions at LEP

Thorsten Wengler¹

CERN, EP-division, 1211 Geneva 23, Switzerland

Received: / Revised version:

Abstract. Jet and di-jet production are studied in collisions of quasi-real photons collected during the LEP2 program at e^+e^- center-of-mass energies from 189 to 209 GeV. OPAL reports good agreement of NLO perturbative QCD with the measured differential di-jet cross sections, which reach a mean transverse energy of the di-jet system of 25 GeV. L3, on the other hand, finds drastic disagreement of the same calculation with single jet production for transverse jet momenta larger than about 25 GeV.

PACS. 13.60.Hb Total and inclusive cross sections (including deep-inelastic processes) – 14.70.Bh Photons – 13.66.Bc Hadron production in e^+e^- interactions

1 Single jet inclusive production

The L3 collaboration [1] has measured inclusive jet production in photon-photon interactions [2]. A total integrated luminosity of 560 pb^{-1} recorded at e^+e^- center-of-mass energies $\sqrt{s_{ee}} = 189 - 209 \text{ GeV}$ is used, with a luminosity weighted average of $\langle \sqrt{s_{ee}} \rangle = 198 \text{ GeV}$. Photon-photon interactions in which one of the electrons is scattered into the detector are rejected, such that both photons are quasi-real. Jets are reconstructed using the k_\perp -clustering algorithm [3] and analysed in the pseudorapidity range $|\eta| < 1$ for jet transverse momenta $3 < p_t < 70 \text{ GeV}$. The remaining background from other processes after event selection increases from about 5% at low p_t to about 20% at high p_t . This background is subtracted bin-by-bin from the data before corrections for selection efficiency and detector acceptance are applied. The differential cross section as a function of p_t is shown in Figure 1. The distribution can be described by a power law function $A p_t^{-B}$ with $B = 3.6 \pm 0.1$. A comparison to a NLO perturbative QCD calculation [4] using the GRV HO parton density functions [5] and $\Lambda^{(5)} = 152 \text{ MeV}$ predicts a much softer spectrum, as can be seen in Figure 1 and fails to describe the data for jet transverse momenta larger than about 25 GeV.

2 Di-jet production and jet structure

OPAL [6] has studied the production of di-jets in the collisions of two quasi-real photons at an e^+e^- centre-of-mass energy $\sqrt{s_{ee}}$ from 189 to 209 GeV, with a total integrated luminosity of 593 pb^{-1} . Di-jet events are of particular interest, as the two jets can be used to estimate the fraction of the photon momentum participating in the hard interaction, x_γ , which is a sensitive probe of the structure of the

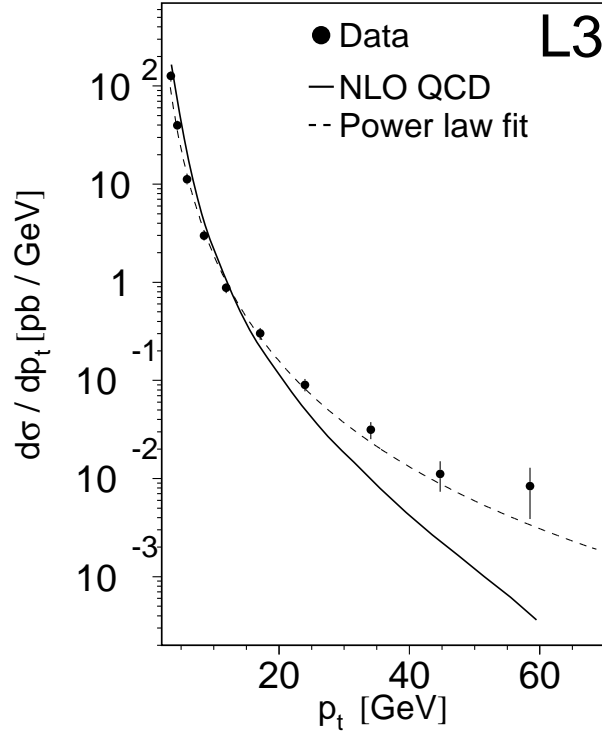


Fig. 1. Inclusive jet differential cross section as measured by L3 compared to NLO perturbative QCD calculations and the result of a power law fit. The theoretical scale uncertainty is less than 20%.

photon. Also here the k_\perp -clustering algorithm [3] is used for the measurement of the differential cross-sections, because of the advantages of this algorithm in comparing to theoretical calculations [7]. The cone jet algorithm is used

to study the different structure of the cone jets compared to jets defined by the k_{\perp} -clustering algorithm.

In LO QCD, neglecting multiple parton interactions, two hard parton jets are produced in $\gamma\gamma$ interactions. In single- or double-resolved interactions, these jets are expected to be accompanied by one or two remnant jets. A pair of variables, x_{γ}^{+} and x_{γ}^{-} , can be defined that estimate the fraction of the photon's momentum participating in the hard scattering:

$$x_{\gamma}^{\pm} \equiv \frac{\sum_{\text{jets}=1,2} (E^{\text{jet}} \pm p_z^{\text{jet}})}{\sum_{\text{hfs}} (E \pm p_z)}, \quad (1)$$

where p_z is the momentum component along the z axis of the detector and E is the energy of the jets or objects of the hadronic final state (hfs). In LO, for direct events, all energy of the event is contained in two jets, i.e., $x_{\gamma}^{+} = 1$ and $x_{\gamma}^{-} = 1$, whereas for single-resolved or double-resolved events one or both values are smaller than 1. Differential cross sections as a function of x_{γ} or in regions of x_{γ} are therefore a sensitive probe of the structure of the photon.

2.1 Jet structure

The internal structure of jets is studied using the jet shape, $\Psi(r)$, which is defined as the fractional transverse jet energy contained in a subcone of radius r in $\eta\phi$ space concentric with the jet axis, averaged over all jets of the event sample. Both k_{\perp} and cone jets are analysed in this way. As proposed in [8], only particles assigned to the jet by the jet finders are considered. Events entering the jet shape distributions are required to have at least two jets with a transverse energy $3 \text{ GeV} < E_{\text{T}}^{\text{jet}} < 20 \text{ GeV}$ and a pseudo-rapidity $|\eta^{\text{jet}}| < 2$.

In Figure 2(a) the jet shape, $\Psi(r)$, is shown for the k_{\perp} algorithm for both $x_{\gamma}^{\pm} > 0.75$ and $x_{\gamma}^{\pm} < 0.75$. The first sample is dominated by direct photon-photon interactions and hence by quark-initiated jets. As is demonstrated in the figure, jets in this sample are more collimated than for small values of x_{γ}^{\pm} , where the cross-section is dominated by resolved processes and hence has a large contribution from gluon-initiated jets. In both cases the jets become more collimated with increasing transverse energy, as is shown in Figure 2(c). There is no significant dependence on the jet pseudo-rapidity (Figure 2(d)). Both PHOJET [9] and PYTHIA [10] give an adequate description of the jet shapes as can be seen in Figures 2(b), (c), and (d). The default choices of SaS1D [11] for PYTHIA and LO GRV [5] for PHOJET are taken. Comparisons of jets defined by the cone algorithm and the k_{\perp} algorithm (not shown here) lead to the conclusion that the behavior described above is similar for both jet algorithms, however cone-jets are significantly broader than the jets defined by the k_{\perp} algorithm at low $E_{\text{T}}^{\text{jet}}$. With increasing $E_{\text{T}}^{\text{jet}}$, jets become more collimated and the two jet algorithms become similar.

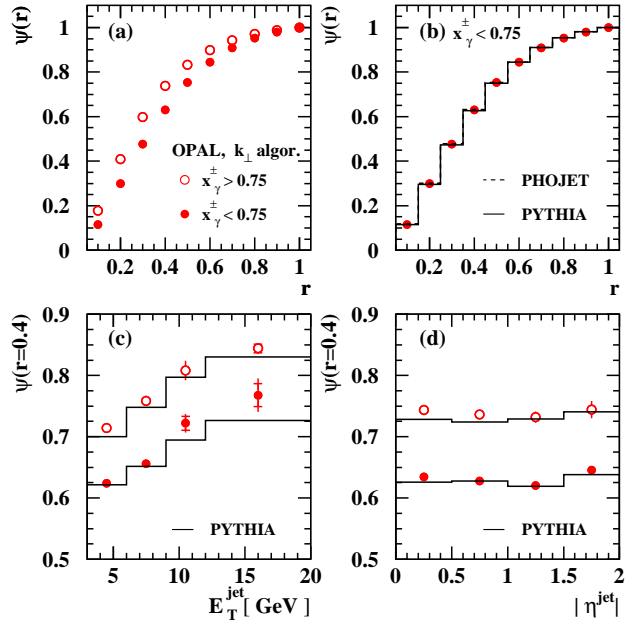


Fig. 2. The jet shape, $\Psi(r)$, for the two regions of x_{γ}^{+} - x_{γ}^{-} -space indicated in the figure (a), and $\Psi(r)$ for $x_{\gamma}^{\pm} < 0.75$ compared to the predictions of the LO MC generators PHOJET and PYTHIA (b). Figures (c) and (d) show the value of $\Psi(r = 0.4)$ as a function of the transverse energy and pseudo-rapidity of the jet respectively, compared to the PYTHIA prediction.

2.2 Differential Di-jet cross-sections

Only the k_{\perp} jet algorithm is used for the measurement of the differential di-jet cross-sections. The experimental results are compared to a perturbative QCD calculation at NLO [12] which uses the GRV HO parametrisation of the parton distribution functions of the photon [5]. The renormalisation and factorisation scales are set to the maximum $E_{\text{T}}^{\text{jet}}$ in the event. The calculation was performed in the $\overline{\text{MS}}$ -scheme with five light flavours and $\Lambda_{\text{QCD}}^{(5)} = 130 \text{ MeV}$. This calculation was shown to be in agreement with the calculation compared to the single inclusive jet measurement above for the di-jet observables presented here [4]. The average of the hadronisation corrections estimated by PYTHIA and HERWIG have been applied to the calculation for this comparison. In the figures described below the shaded band indicates the theoretical uncertainty estimated by the quadratic sum of two contributions: variation of the renormalisation scale by factors of 0.5 and 2 and the difference between using HERWIG or PYTHIA in estimating the hadronisation corrections.

The differential di-jet cross-section as a function of the mean transverse energy $\bar{E}_{\text{T}}^{\text{jet}}$ of the di-jet system is shown in Figure 3. At high $\bar{E}_{\text{T}}^{\text{jet}}$ the cross-section is expected to be dominated by direct processes, associated with the region $x_{\gamma}^{\pm} > 0.75$. Consequently we observe a significantly softer spectrum for the case $x_{\gamma}^{\pm} < 0.75$ than for the full x_{γ}^{+} - x_{γ}^{-} -space. The calculation is in good agreement with the data for the full x_{γ}^{+} - x_{γ}^{-} -range and for x_{γ}^{+} or $x_{\gamma}^{-} < 0.75$.

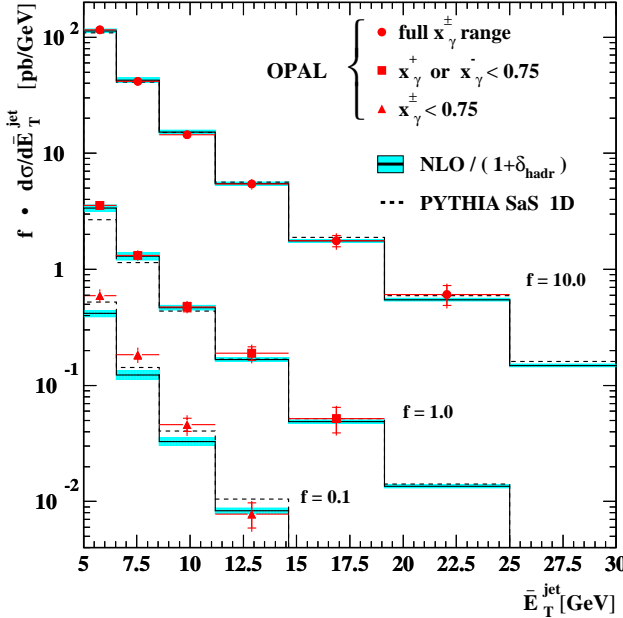


Fig. 3. The di-jet cross-section as a function of the mean transverse energy \bar{E}_T^{jet} of the di-jet system, for the three regions in $x_\gamma^+ \text{-} x_\gamma^-$ -space given in the figure. The factor f is used to separate the three measurements in the figure more clearly.

The cross-section predicted for $x_\gamma^\pm < 0.75$ is below the measurement. It should be noted that in this region the contribution from the underlying event, not included in the calculation, is expected to be largest, as shown below. PYTHIA 6.161 is in good agreement with the measured distributions using the SaS1D parton densities. PYTHIA includes a model of the underlying event using multiple parton interactions (MIA).

The three plots of Figure 4 show the differential cross section as a function of x_γ for the three regions in $x_\gamma^+ \text{-} x_\gamma^-$ -space described above. The shaded histogram on the bottom of each of the three plots indicates the contribution of MIA to the cross section as obtained from the PYTHIA [10] MC generator. It is evident especially for $x_\gamma^\pm < 0.75$ that the MIA contribution is of about the same size as the discrepancy between the measurement and the NLO prediction. Furthermore it is interesting to observe that there is next to no MIA contribution to the cross section if either x_γ^+ or x_γ^- is required to be less than one, while the sensitivity to the photon structure at small x_γ is retained. As one would expect also the agreement of the NLO calculation with the measurement is best in this case. For large x_γ the NLO calculation does not agree well with the data. However, it has been pointed out that the calculation of the cross section becomes increasingly problematic when approaching $x_\gamma = 1$ [4, 13].

With these measurements one is therefore able to disentangle the hard subprocess from soft contributions and make the firm statement that NLO perturbative QCD is adequate to describe di-jet production in photon-photon collisions in the regions of phase space where the calculation can be expected to be complete and reliable, i.e.

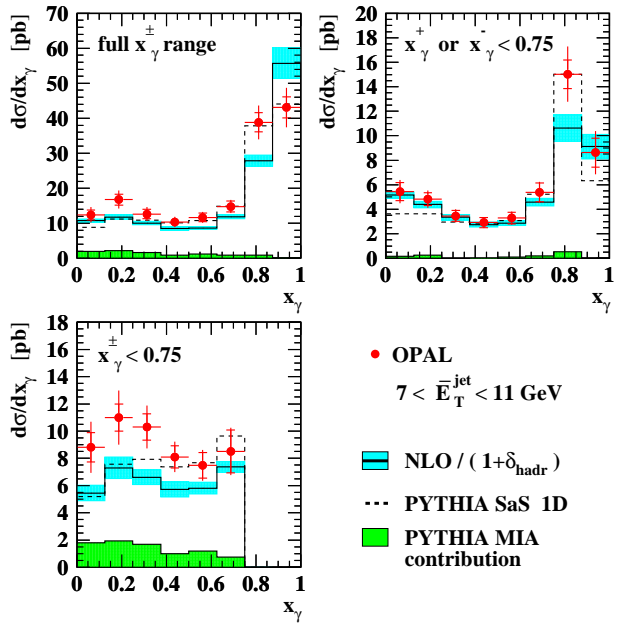


Fig. 4. The di-jet cross-section as a function of x_γ and for the regions of the mean transverse energy \bar{E}_T^{jet} and x_γ^\pm of the di-jet system indicated in the figures.

where MIA contributions are small and for x_γ not too close to unity. At the same time a different sub-set of observables can be used to study in more detail the nature of the soft processes leading to the underlying event.

References

1. L3 Collaboration, B. Adeva et al., Nucl. Instrum. Methods A289 (1990) 35.
2. L3 Collaboration, P. Achard et al., CERN-EP/2003-055, Submitted to Physics Letters B.
3. S. Catani, Yu.L. Dokshitzer, M.H. Seymour, B.R. Webber, Nucl. Phys. B406 (1993) 187; S.D. Ellis, D.E. Soper, Phys. Rev. D48 (1993) 3160.
4. L. Bertola, S. Frixione, Proceedings of Photon '03, Frascati, Italy, 7-11 April 2003, edited by F. Anulli, S. Braccini, G. Panzeri, to be published in Nucl. Phys. B; hep-ph/0306167.
5. M. Glück, E. Reya, A. Vogt, Phys. Rev. D45 (1992) 3986; M. Glück, E. Reya and A. Vogt, Phys. Rev. D46 (1992) 1973.
6. OPAL Collaboration, K. Ahmet et al., Nucl. Instrum. Methods A305 (1991) 275.
7. M. Wobisch, T. Wengler, hep-ph/9907280; M.H. Seymour, hep-ph/9707349; S.D. Ellis, Z. Kunszt, D.E. Soper, Phys. Rev. Lett. 69 (1992) 3615.
8. M.H. Seymour, Nucl. Phys. B513 (1998) 269.
9. R. Engel, Z. Phys. C66 (1995) 203; R. Engel, J. Ranft, Phys. Rev. D54 (1996) 4244.
10. T. Sjöstrand, Comp. Phys. Comm. 82 (1994) 74; T. Sjöstrand, LUND University Report, LU-TP-95-20 (1995).
11. G.A. Schuler, T. Sjöstrand, Z. Phys. C68 (1995) 607.
12. M. Klasen, T. Kleinwort, G. Kramer, Eur. Phys. J. Direct C1 (1998) 1; B. Pötter, Eur. Phys. J. Direct C5 (1999) 1.
13. M. Klasen, Rev. Mod. Phys. 74 (2002) 1221.